Chapter 6

Giant Meta-magnetism behavior in double perovskite material $Y_{2-x}Ca_xCoMnO_6$ (x=0.10, 0.20)

6.1. Introduction

The term 'perovskite' derives from the mineral $CaTiO_3$. Gustav Rose found this mineral in the Ural. Mountains of Russia in 1839 and named after Russian mineralogist Lev Perovski. Such multifunctional features of completely correlated oxide materials often result from the coexistence of coupled microscopic degrees of freedom, such as phonon, polarization, and spin [199–202]. Thus, the need for such materials has recently gained momentum to harness their unique properties to develop advanced applications such as spin filters, memory devices, capacitive devices, and, spin switching among others [203–205]. Double perovskite (DPs), discovered in the first decade of the 1950s, are especially fascinating complex oxides that have continued to attract the scientific community's interest concerning both applications and basic knowledge. DPs have a structure with double the unit cell of perovskite, and their unique formula is $R_2\ BB'O_6$. Each of the eight holes left behind by the $BO_6/B'O_6$ octahedral are filled

with a cation, typically an alkaline earth or rare-earth metal ion that is 12 times more coordinated to Oxygen. They contain fascinating properties like exchange bias (EB) [7], Magneto-dielectric, Magneto-capacitance, Magneto-caloric effect, and others, which account for applications in sensors, spintronic, energy harvesting devices, transformers, and tunable microwave filters [168,168,170,200,200,206–209]. Such intriguing multifunctional properties result from the robust interaction between lattice degree of freedom, spin, and charge. The presence of the meta-magnetic phase transition in a variety of complex magnetic systems has recently reopened fascination with the field of research. This phenomenon is characterized by sudden jumps in magnetization in response to external disturbances such as changes in the magnetic field, temperature, and pressure. Since a lot of DPs with 'A' site nonmagnetic cations alike Eu, Y, La, and Lu demonstrate the most fascinating property of the isothermal magnetization graph, the meta-magnetic transition [208,209]. In recent years, meta-magnetic behavior has also been reported in some of the most well-known Multiferroic systems, such as $BiFeO_3$ and phase-separated multi-ferroic $Eu_{1-x}Y_xMnO_3$(x = 0.20, 0.25) systems. An interesting coupling between meta-magnetic behavior and ferroelectric polarization with the applied field has been observed. Recently, improper magnetic multiferroicity was predicted for Y_2NiMnO_6 and experimentally observed in the double perovskite systems Lu_2CoMnO_6 [17] and Y_2CoMnO_6 [18], where the E*-type AFM ordering with collinear spin structure affects the spatial inversion symmetry and leads to spontaneous polarization. An initial study on Y_2CoMnO_6 demonstrated that there is significant FM hysteresis including meta-magnetic "steps" below 8 K [19]. We utilized a model for the pinning of magnetization at the anti-phase boundaries caused by antisite disorder to explain the existence of "steps" in magnetic hysteresis. These jumps referred to martensitic transformations [20] observed in inter-metallic and demonstrated first-order features [14]. The combined presence of AFM and ferroelectric ordering is of major significance in spintronic and data storage applications.

We focused on the magnetic features of Y_2CoMnO_6 with Ca^{2+} substitution at the Y site by 5% and 10%. The Ca^{2+} replacement could lead to an electron transfer between the Ca^{2+} ions and the transition ions (Mn and Co ions), which would also vary the valence states of Mn and Co cations. It could change the nature of magnetic ordering. Thus, in the YCCMO5 and YCCMO10 system, AFM coupling of Mn^{3+} - O^{2-} - Co^{3+} and FM coupling of Mn^{4+} - O^{2-} - Co^{2-} coexists. The dominating magnetization of the YCCMO5 and YCCMO10 systems is subject to change when the Ca^{2+} substitution takes place. Furthermore, the saturation magnetization (M_S) and T_C of the samples fall with increasing Ca^{2+} substitution, while the exchange bias value increases. In this paper, we demonstrate the field-dependent sudden magnetization steps that occur in the YCCMO5 and YCCMO10 polycrystalline samples at low temperatures, suggesting a martensite-like scenario.

6.2. Sample preparation

The starting components (highly pure at 99.98%) Y_2O_3, Cao, CoO, and Mn_2O_3 were mixed in the perfect ratios and crushed for 70 minutes before they were heated in the atmosphere for 25 hours at 950 ℃. After getting it to ambient temperature, it was crushed again for 20 minutes before being heated for 36 hours at 1050 ℃. A second heat treatment was carried out at 1150 and 1250 ℃. Reground from the resultant powder, the pellets had dimensions between 2 mm and 3 mm in width and 10 and 11 mm in circumference. These pellets were sintered at 1350 ℃ for 45 hours. It was then proceeded to cool to room temperature (0.8 ℃ /min.) to avoid pellet fractures. X-ray diffraction (XRD) was measured using a ground-up piece of the sintered pellet.

6.3. Result and discussion

6.3.1. Structure analysis

V.M. Goldschmidt initially identified the crystal structure and created the tolerance factor theory. The B and B′ cations' different ionic sizes have significant effects on how these cations arrange themselves. Therefore, the stability of samples is the most significant factor of the perovskite structure. To explain the stable structure of Perovskite, the Goldschmidt tolerance factor (t) is an essential variable [210]. The Goldschmidt tolerance factor for mixed A-site $A_{2-x}A'_xBB'O_6$ Double perovskite, which can be calculated by the equation, can be used to determine the stability of the crystal [211],

$$t = \frac{\frac{(2-x)r_A+(x)r_{A'}}{2}+r_O}{\sqrt{2}\left(\frac{r_B+r_{B'}}{2}+r_O\right)} \quad (36)$$

Where r_A, $r_{A'}$, and r_B, $r_{B'}$, are the Shannon radii of A and B site ions, correspondingly and r_O is the Shannon radius of O^{2-}.The tolerance factor varies between pure and a YCCMO5 and YCCMO10 doped sample, ranging from 0.76 to 0.81 for monoclinic structure [211]. Crystalline YCCMO5 and YCCMO10 sample powder x-ray diffraction data have been collected for structural characterization. In the FULLPROF code, the Rietveld method [212] is used to evaluate the observed X-ray diffraction pattern. YCCMO5 and YCCMO10 exhibit a monoclinic structure of the P21/n space group as shown in Fig 6.1 [134].

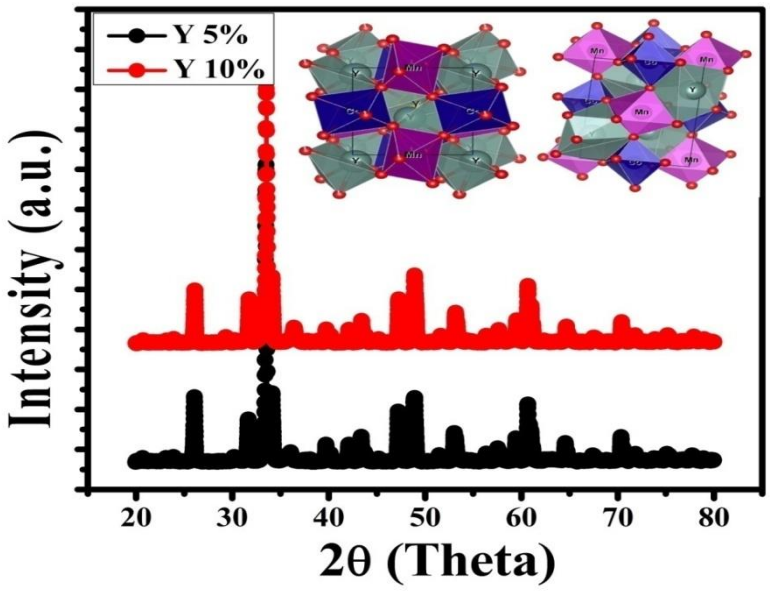

Figure 6.1: *The X-ray diffraction pattern utilizing Rietveld refinement and the structure of YCCMO 5 and YCCMO10 with an inset showing the 3D structure of samples.*

YCCMO5	x	y	z	Angle and lattice parameter
Y	0.52166	0.57535	0.26044	a =5.2513 Å
Ca	0.52166	0.57535	0.26044	b =5.6508 Å
Co	0.00000	0.50000	0.00000	c =7.4406 Å
Mn	0.50000	0.00000	0.00000	$\alpha = 90.000^0$
O1	0.39005	0.95420	0.22806	$\beta = 89.998^0$
O2	0.33361	0.33020	0.06371	$\gamma = 90.000^0$
O3	0.24040	0.77614	0.04211	
Reliability factor $(\chi)^2 = 3.55$, Tolerance factor (t) = 0.77, Direct Cell Volume (V) = 220.79 $Å^3$				

YCCMO10	x	y	z	Angle and lattice parameter
Y	0.51629	0.57537	0.26134	a = 5.25446 Å
Ca	0.51629	0.57537	0.26134	b = 5.63908 Å
Co	0.00000	0.5000	0.0000	c = 7.43876 Å
Mn	0.50000	0.0000	0.0000	$\alpha = 90.000^0$
O1	0.39456	0.95963	0.23377	$\beta = 89.994^0$
O2	0.33151	0.33967	0.06531	$\gamma = 90.000^0$
O3	0.23606	0.78684	0.05362	
Reliability factor $(\chi)^2 = 4.8971$, Direct Cell Volume (V) = 220.413 $Å^3$ Tolerance factor (t) =0.78				

6.3.2. X-ray Photoemission Spectroscopy analysis

It is essential to be familiar with the electrical structures of the given systems before understanding their magnetic properties [170]. The National Institute of Standards and Technology (NIST) XPS database was used to assign all peak positions and peak separations in the collected data [180]. Except for C, no other impurity elements were discovered in the spectra as shown in Fig 6.2(a) and 2(d). The occurrence of the C1s peak corresponds to the casual molecules that were absorbed at the surface level from the atmosphere. The Y(3d) region's spin-orbit split peaks, Y-$3d_{3/2}$ and Y-$3d_{5/2}$, are seen in core-level XPS measurements of both pure YCCMO5 and YCCMO10 samples at energies of 158.7 eV and 156.7 eV, separately, with peak separation of 2.1 eV [213]. Core-level spectra of the Mn (2p) in the YCCMO5 and YCCMO10 samples reveal that the spin-orbit coupling (ΔE) of the peaks Mn-$2p_{1/2}$ and Mn-$2p_{3/2}$ is determined to be near 11.7 eV as displayed in Fig 6.2(b) and 2(c). The values of ΔE for Mn (2p) XPS spectrum in MnO_2 and Mn_2O_3 are about 11.8 eV, and 11.6 eV, separately [185]. The mixed-valence (+3 and +4) oxidation states of Mn ions may be indicated by the in-between value of the ΔE for the current system, which agrees with earlier reports on comparable systems [214]. Furthermore, the observed Mn (2p) XPS spectrum shows satisfactory agreement with other identical systems that contain Mn ions in mixed oxidation states (+4/+3) in terms of peak positions and line forms [186,187].The XPS examination of the Co-containing system is especially significant because their spectra include satellite peaks in addition to the primary photoelectron lines, which are extremely sensitive to oxidation states, legend coordination, and other factors. The core-level Co(2p) spectra of the YCCMO5 and YCCMO10, which include the Co-$2p_{1/2}$ and Co-$2p_{3/2}$ peaks that are spin-orbit split, are displayed in Fig 6.2(e) and 2(f). Therefore, it is discovered that the Co(2p) peak separation (E) for YCCMO5 is around 15.5 eV whereas for YCCMO10 it drops to 15.1 eV [215]. In reality,

it is stated that the Co(2p) doublet separation in the mixed +3 and +2 states of Co_3O_4 and CoO (divalent Co) is 15.3 eV and 15.9 eV, separately [115,123].

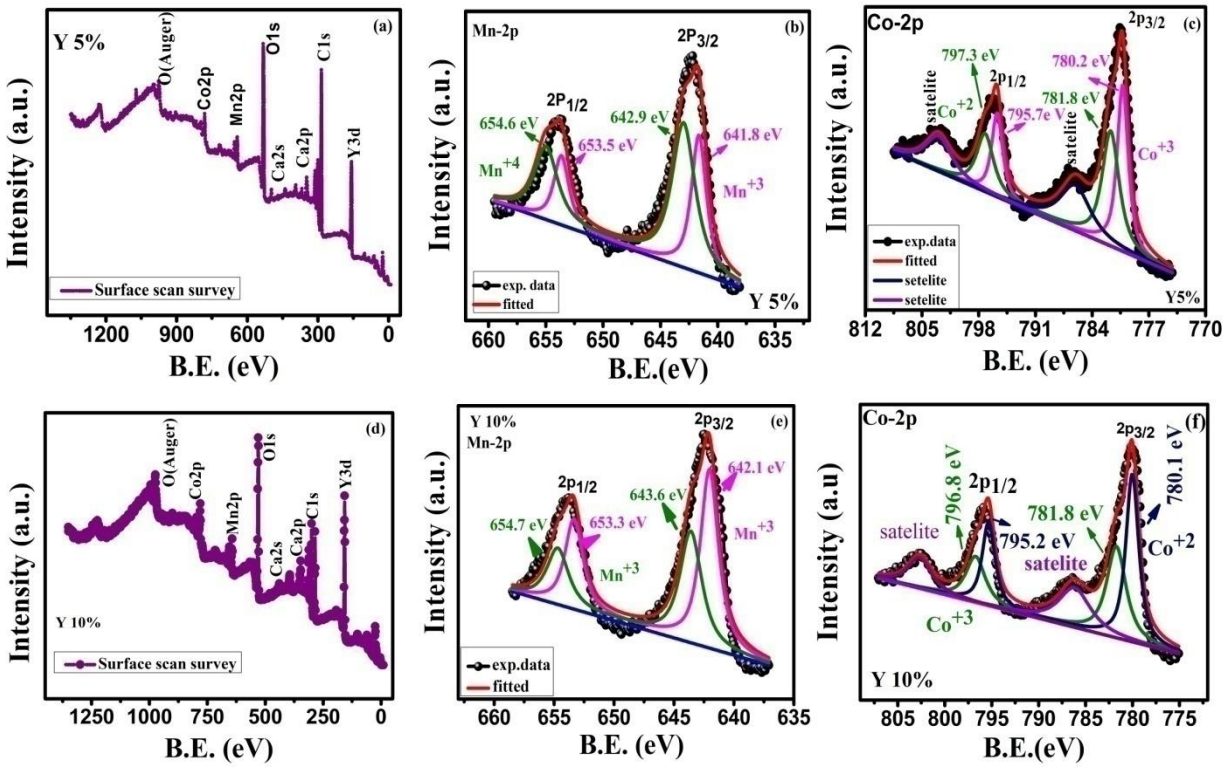

Figure 6.2: *(a)–(c) Surface scan & core-level XPS of different elements of both samples YCCM5 and (d)-(f) shows YCCMO10.*

This shows that the Co cations belong in mixed +2/+3 valence states in both the YCCMO5 and YCCMO10 samples. However, because of the higher oxidation states of Co driven on by Ca doping, a decrease in doublet separation has been observed. The XPS findings confirm our XRD and magnetometer findings about the valence state of the Mn and Co ions in the sample, which may be explained in terms of a mixed valence state of Co^{2+} and Co^{3+} [216].

6.3.3. Resistivity vs. temperature

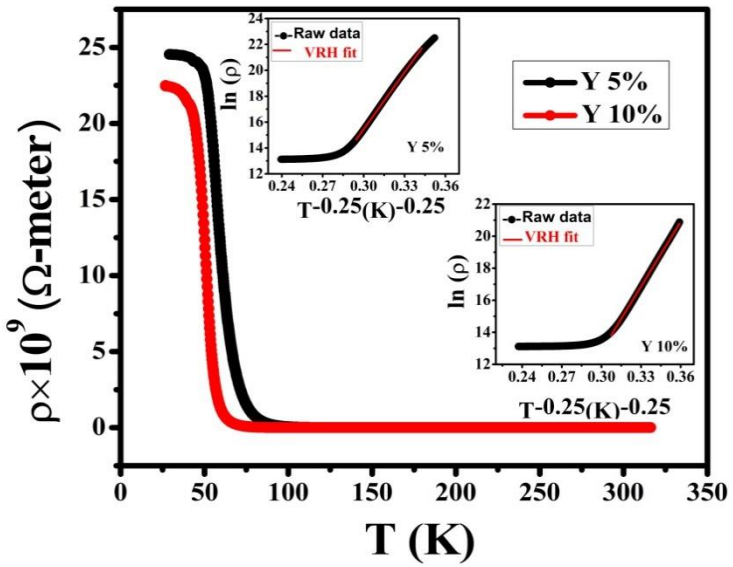

Figure 6.3: *(a) The temperature-dependent resistivity of YCCMO5 and YCCMO10, with insets showing VRH model fitting.*

The curve of electrical resistivity (ρ) *vs.* temperature (T), with resistance 12×10^9-1×10^9 Ohm, for the perovskite YCCMO5 and YCCMO10 in the temperature domain of 50—300 K, can be used to observe the insulating /semiconducting behavior of the material as shown in Fig 6.3. As Ca-substitution is increased while the temperature remains constant (as seen in Fig.6.3), the resistivity increases. Due to the high resistance of the compound and the limit of our measurement system resistivity measurements below 40 K were not possible. However, we divide the data on resistivity into two temperature ranges: the insulating range, 40–70 K, and the semiconducting range, 70–300 K. The VRH model can be used to explain the variation in resistivity for both systems below 200 K. It was mentioned that structural defects, oxygen vacancies, or cation disorder, can create an impurity band near the Fermi level, and localization of electrons in the impurity band could happen in VRH-type conduction. Variable range hopping (VRH) is described by the equations

$$\rho = \rho_0 \exp\left(\frac{T_0}{T}\right)^{1/4} \qquad (37)$$

$$ln\rho = ln\rho_0 + T_0^{1/4}.\, T^{-1/4} \quad (38)$$

Where T_0, also called the Mott's characteristics temperature, is a crucial factor in establishing the transport features of the system and ρ_0 is a pre-factor [67]. Where T_0 is Mott's characteristic temperature, which governs the system's electrical transport properties, and ρ_0 refers to pre-factor.T_0 is given as,

$$T_0 = \frac{24\alpha^3}{\pi K_B N E_F} \quad (39)$$

Where (1/α) is the localization length of the wave function. N(EF) is the density of the localized state near the Fermi level [67]. The numerical value of T_0 is calculated from the inclination of the fitted line with equation (39), $T_0 = 1.3\times10^9$. The length of the localization (1/ α) is twice that of the Mn-Co bond length in numbers as well. At temperature T, the equation can be used to calculate the polaron activation energy (w).

$$W = \frac{1}{4}\left(K_B T_0^{1/4} T^{3/4} \right) \quad (40)$$

With the most possible hopping distance

$$R = \left[\frac{9}{8\Pi\alpha K_B N E_F}\right]^{1/4} = \left[\frac{9T_0}{192\alpha^4}\right]^{1/4} \quad (41)$$

For the systems at the Fermi level, the value of N (EF) was determined to be approximately ~10^{24} eV^{-1} m^{-3}, which is comparable to the value of a classic semiconductor oxide.

6.3.4. Magnetization measurement

Fig 6.4(a) and 4(b) demonstrate the thermal variations of the DC magnetization (M) graphs utilizing the usual field-cooled (FC) and zero-field cooled (ZFC) procedures with an applied field of 100 Oe in the temperature domain of 2-300 K for the samples YCCMO5 and YCCMO10, separately.

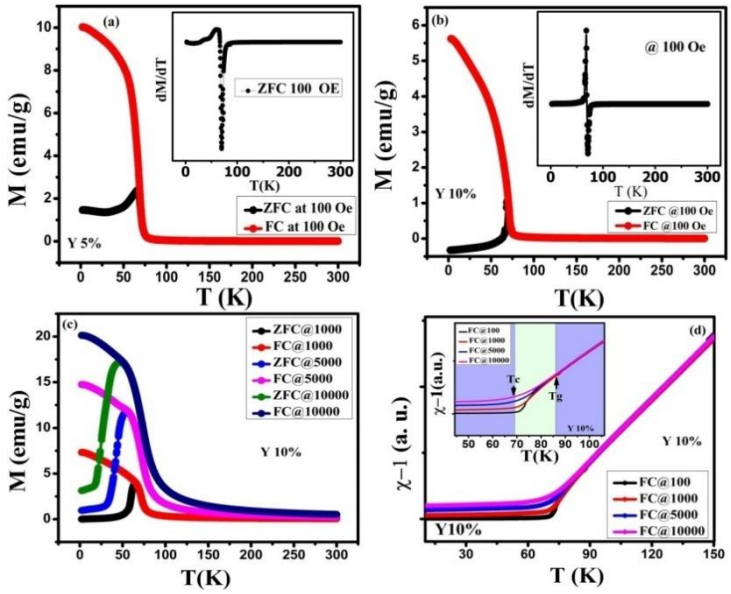

Figure 6.4: *(a), (b) The temperature-dependent magnetization curves at two different applied ZFC and FC conditions. Inset: showing the derivative of the MZFC–T curve with inset showing the variation of T_C of YCCMO5 and YCCMO10 respectively. (c) The ZFC/FC magnetization of YCCMO10 at 1 kOe, 5 kOe, and 10 kOe applied field. (d) The temperature-dependent inverse susceptibility curves at different fields of YCCMO10.*

It has been suggested that the complex magnetic interaction among rare earth cation and transition metal lattices is responsible for of magnetization decrease in ZFC curves below 80 K. It is referred to that the magnetization features of DP's are significantly affected by the mixed-valence states of Mn and Co cations and the ASD due to a varies of the B-O-B′ exchange interaction. Based on the derivation of the magnetization dM/dT, the Tc in these systems is estimated to be 70 K for YCCMO5 and 68 K for YCCMO10. The T_C, however, is quite lower than the parent compound YCMO has 75 K [199]. Unlike the YCMO sample, the Ca-doped samples exhibit a magnetic transition Tc that has sharply dropped as the quantity of Co^{3+} ions increased at the expense of Co^{2+} ions. The observed reduction in the magnitude of the M (T) with increasing Ca substitution can be argued by the introduction of the competing AFM super-exchange interaction via Co^{3+}–O^{2-}–Co^{2+}, Co^{3+} –O^{2-}–Co^{3+}, and so on. It should be noted that the

ZFC curve for YCCMO10 at lower temperatures showed an insignificant but negative value of M (T) with an applied field of 100 Oe. We confirmed zero residual fields before repeating the experiments, which provided the same results, eliminating the possibility of instrument errors [2]. However, negative magnetization at the low field is frequently observed in similar DP compounds. This can be explained by the presence of anti-parallel spins and/or canted ferromagnetic domains or clusters that are separated by the anti-phase boundary, which is brought about by ASD [217].

The ZFC and FC graphs demonstrate a significant bifurcation, with the amplitude of the bifurcation increasing as the applied field rises from 1 kOe to 10 kOe in both samples. The bifurcation may be a sign of a usual spin-glass phase. It is not a necessary characteristic of a typical spin-glass, as it can also result from the domain structure of a ferromagnetic material or magnetic anisotropy [76]. In a lot of FM materials, the ZFC and FC M(T) graphs usually bifurcate, which outcomes via magnetic anisotropy [218]. Due to the suppression of magnetic anisotropy in the high field, the bifurcation should occur at a lower temperature in a higher magnetic field, which was also observed in YCCMO5 and YCCMO10. In the YCCMO5 and YCCMO10, respectively, ZFC M (T) exhibits a small tapered maximum with a cusp at Ta ~ 69.5 K and ~ 68.3 K at 100 Oe field. Ta is the temperature at which anisotropy energy and the energy brought on by the applied field are almost of equal magnitude. These cusps also exhibit a plateau-like anomaly, a change in cusp temperature (Ta) towards lower temperature as the magnetic field increases (H), and Ta α H at higher magnetic fields (1 kOe, 5 kOe, and 10 kOe). This might be a result of a conflict between the local anisotropy and the influence of the applied magnetic field [90].

6.3.5. DC susceptibility

The YCCMO5 and YCCMO10 have inverse DC susceptibility (-1/χ) at the constant magnetic field that varies with temperature as seen in Fig 6.5. Above 100 K, the χ^{-1}(T) demonstrates a linear temperature dependence, indicative of a paramagnetic phase following the Curie-Weiss (CW) law, i.e.,

$$\frac{1}{\chi} = \frac{T}{C} - \frac{T_{CW}}{C} \tag{42}$$

$$C = \frac{N\mu_{eff}^2}{3K_B} \tag{43}$$

We calculated the effective magnetic moment of 5.4 μ_B And the C-W temperature (T_{CW}) of 68 K for the YCCMO5 based on the CW fitting. According to estimates, the effective magnetic moment and T_{CW} for YCCMO10 were around 5.7 μ_B And 64 K, whereas they were approximately 3.9 μ_B And 80 K for YCMO. A positive value for T_{CW} indicates that ferromagnetic interactions are dominant [134].

6.3.6. Magnetic hysteresis graph

Fig 6.6 shows the isothermal magnetization of YCCMO5 and YCCMO10 that was taken at 2, 60, and 300 K. At 2 K, the magnetization isotherms have distinct steps, but as the temperature rises, the steps will disappear [208].

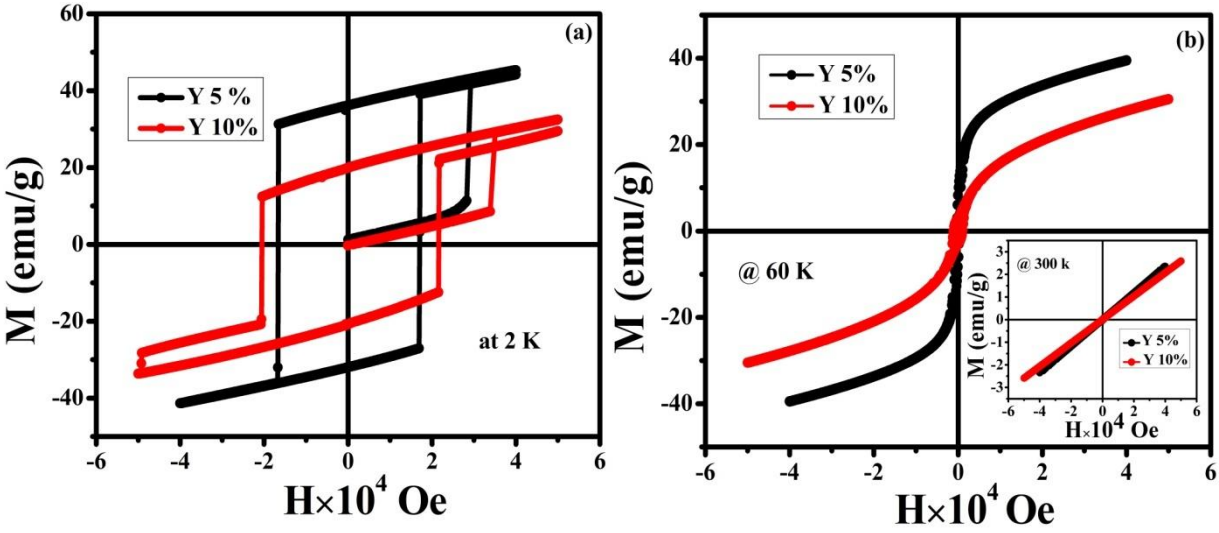

Figure 6.5: *(a) The isothermal magnetizations vs. magnetic field of YCCMO5 and YCCMO10 at different temperatures at 2 K. (b) shows at 60 K and its inset shows 300 K.*

Due to slow spin relaxation, these jumps are only visible in the rising field, from 0 to 5 Tesla, and are absent in the falling field, from 5 to 0 Tesla. They reappear in the following negative field direction, from 0 to -5T, and are supported by large remanence and coercivity. The presence of the virgin graph outer of the original M-H close curve is another feature of the hysteresis close curve. The virgin loop is outside at T = 2 and 60 K, but it is enclosed inside the original M-H close curve at higher temperatures. According to Manekar et al. for Ce $(Fe_{0.96}Al_{0.04})_2$, the virgin curve emerging from the main hysteresis loop provides additional proof that dynamics in a spin system have been frozen [219]. In Y_2CoMnO_6 [208] and Eu_2CoMnO_6 [76] both sample shows the metamagnetic state at 2 K-5 K while at 8k it will disappear. The steps in the hysteresis curve will disappear when higher field cooling data is taken. It has been attempted to explain the meta-magnetic transition (MMT) in Y_2CoMnO_6 by the field-influence spin reorientation of the Mn and Co ions [220,221]. Some Multiferroic materials, such as Ca_3CoMnO_6 [222–224], are thought to have field-induced sharp jumps that are caused by spin flop transitions from E*-type magnetic ordering (↑↑↓↓) to the (↑↑↑↓) Mn^{4+}

(high spin state, S = 3/2) at first critical field H_{C1} and to (↑↑↑↑) with Co^{2+} (low spin state, S = 1/2) at second critical field H_{C2}. In addition, these abrupt jumps in magnetization may be the result of spin flopping and field-influenced lattice deformation (martensitic-alike transition), which result in the transition between the FM and AFM phases and are observed for a range of critical values of the applied field.

6.4. Conclusion

In conclusion, samples of double perovskite polycrystalline YCCMO5 and YCCMO10 were produced utilizing the usual solid-state reaction process. At ambient temperature, the structure of the system is monoclinic with the space group P21/n. The XPS measurement shows that Co and Mn ions exist in a mixed state. Semiconducting-like behavior is observed in the resistivity of YCCMO (5%, 10%) samples, and Mott's three-dimensional VRH and SPH models provide a good fit for the nature of electrical conduction. The double perovskite YCCMO5 and YCCMO10 display ferromagnetic transition at Tc ~70 K and Tc ~ 68 K. Isothermal field-dependent magnetization shows meta-magnetic behavior at low-temperature regions in both samples but the magnitude of meta-magnetic decreases in YCCMO10 due increased Ca ion at Y site witch decreases magnetic interaction between transition metal ion. YCCMO10 also has a Griffith-like phase above the transition temperature